Magnetorotational instability of dissipative Couette flow

Jeremy Goodman and Hantao Ji

Princeton University Observatory, Princeton, NJ 08544

jeremy@astro.princeton.edu

ABSTRACT

Global axisymmetric stability of viscous, resistive, magnetized Couette flow is re-examined, with the emphasis on flows that would be hydrodynamically stable according to Rayleigh's criterion: opposing gradients of angular velocity and specific angular momentum. In this regime, magnetorotational instabilities [MRI] may occur. Previous work has focused on the Rayleigh-unstable regime. To prepare for an experimental study of MRI, which are of intense astrophysical interest, we solve for global linear modes in a wide gap with realistic dissipation coefficients. Exchange of stability appears to occur through marginal modes. Velocity eigenfunctions of marginal modes are nearly singular at conducting boundaries, but magnetic eigenfunctions are smooth and obey a fourth-order differential equation in the inviscid limit. The viscous marginal system is of tenth order; an eighth-order approximation previously used for Rayleigh-unstable modes does not permit MRI. Peak growth rates are insensitive to boundary conditions. They are predicted with surprising accuracy by WKB methods even for the largest-scale mode. We conclude that MRI is achievable under plausible experimental conditions using easy-to-handle liquid metals such as gallium.

1. Introduction

To an even greater extent than large-scale terrestrial ones, astrophysical flows are nearly inviscid. Yet observations show that they dissipate efficiently. For example, accretion disks (flattened systems of gas in orbit about a star or black hole) must lose orbital energy in order that the gas flow onto the central object. The influence of turbulence has long been suspected, but purely hydrodynamic turbulence is probably ineffective because of the strongly stable radial angular momentum gradient in the disk. When warm enough to be partially ionised, as they often are, accretion disks become magnetohydrodynamic (MHD) fluids. It is now believed that turbulence and orbital decay are driven by magnetorotational instabilities (MRI). Although discovered by Velikhov (1959) and Chandrasekhar (1960), MRI did not come to the attention of the astrophysical community until rediscovered by Balbus & Hawley (1991). MRI requires that the angular velocity (Ω) must decrease with distance from the axis, but it is distinguished from Rayleigh's centrifugal instability by persisting when the gradient of specific angular momentum is positive, *i.e.* $\partial(r^4\Omega^2)/\partial r > 0$. A

weak background magnetic field is required, and MRI can be axisymmetric when the field parallel to the rotation axis. The rotation law of accretion disks satisfies both conditions above (usually $\Omega \propto r^{1/2}$), and while the magnetic geometry is uncertain, it has little influence on the maximum MRI growth rate in ideal MHD unless the field is purely toroidal (Balbus & Hawley 1992; Terquem & Papaloizou 1996).

There exists a body of experimental work on magnetized Couette flow (Donnelly & Ozima 1960, 1962; Donnelly & Caldwell 1964; Brahme 1970), but the MRI has never been demonstrated in the laboratory. The main obstacle is that liquid metals are strongly resistive on laboratory scales, with magnetic diffusivity $\eta \gtrsim 10^3$ cm^2 s^{-1}. The viscosity is much smaller, typically $\nu \sim 10^{-3}$ cm^2 s^{-1}. Their ratio is the magnetic Prandtl number $P_{\rm m} \equiv \nu/\eta \sim 10^{-6}$.

Chandrasekhar (1961) also analyzed *dissipative* magnetized Couette flow. After laying out general equations for viscous and resistive linearized axisymmetric perturbations, he discarded a term involving shear from the azimuthal induction equation on the grounds that $P_{\rm m} \ll 1$. In fact the neglected term involves neither ν nor η directly. Thus the commonly used name "small-$P_{\rm m}$ approximation" is somewhat unfortunate. It presumes that viscous and inertial forces are comparable throughout the flow. Although this is often the case for marginal Rayleigh instabilities resisted by viscous (and perhaps magnetic) forces, it is not the case for the MRI modes of interest here, where viscosity is important in boundary layers only. We shall show that MRI modes do not exist in Chandrasekhar's approximation (§3).[1] We shall introduce a different $P_{\rm m} \to 0$ limit that retains all terms in the induction equation but neglects viscous boundary layers.

Chandrasekhar's results have been refined by Chang & Sartory (1967); Hassard, Chang, & Ludford (1972); Vislovich, Novikov, & Sinitsyn (1986); Takhar, Ali, & Soundalgekar (1989); Soundalgekar, Ali, & Takhar (1994); Chen & Chang (1998), but always under Chandrasekhar's "small-$P_{\rm m}$" approximation.

In a previous paper (Ji, Goodman, & Kageyama 2001, henceforth Paper I), we have used local WKB methods to survey the MRI regime for realistic materials and laboratory parameters. The most unstable modes (and perhaps the only ones accessible to experiment in the near term) have wavelengths twice as large as the apparatus, so that WKB methods are not to be trusted *a priori*. The present paper therefore discusses the global linear analysis. We integrate the full set of viscous and resistive equations *via* an initial-value scheme to obtain numerical growth rates for cases that would be stable by Rayleigh's criterion. Boundary conditions are problematic for inviscid marginal modes. Nevertheless, the locally obtained growth rates are found to be good approximations, even though the radial eigenfunctions are far from being sinusoidal. We predict instability under feasible conditions: gap widths and heights of order ten centimeters, fields strengths of several kilogauss, and rotation rates of several hundred radians per second.

A supplementary analysis shows that curves of marginal MRI stability are well approximated

[1]Of course he did find MRI modes, but in a separate analysis assuming ideal MHD(Chandrasekhar 1960).

by completely neglecting viscous terms, especially for insulating cylinders. Although $P_{\rm m} \to 0$, this is *not* Chandrasekhar's approximation. It eliminates the velocity perturbations from the analysis and leads to a system of only four radial derivatives. The boundary conditions on velocity are not satisfied by the reduced system even with stress-free (slipping) boundaries. This is resolved by restoring the viscosity but there is little change in the magnetic eigenfunctions or the growth rate when $P_{\rm m}$ is realistically small. Hence when MRI are of primary interest, dimensionless numbers based on viscosity, *viz.* Hartmann and Taylor numbers, are less useful for characterizing stability than numbers that remain finite as $P_{\rm m} \to 0$, such as Lundquist number and magnetic Reynolds number.

2. Basic equations and boundary conditions

We use cylindrical coordinates $r\theta z$ aligned with the rotation of the fluid, and gaussian electromagnetic units. In equilibrium, the magnetic field is constant and parallel to the axis; it is described by the associated Alfvén speed $V_A \equiv B_0/\sqrt{4\pi\rho}$, where ρ is the (constant) density of the liquid metal. The angular velocity is $\Omega(r)$. Perturbations are axisymmetric and sinusoidal in z with wavelength $2\pi/k$:

$$\begin{array}{rclrcl} \delta B_r/\sqrt{4\pi\rho} &=& \beta_r(r,t)\cos kz & \delta v_r &=& \varphi_r(r,t)\sin kz \\ \delta B_\theta/\sqrt{4\pi\rho} &=& \beta_\theta(r,t)\cos kz & \delta v_\theta &=& \varphi_\theta(r,t)\sin kz \\ \delta B_z/\sqrt{4\pi\rho} &=& \beta_z(r,t)\sin kz & \delta v_z &=& \varphi_z(r,t)\cos kz \end{array} \tag{1}$$

We often write $h \equiv \pi/k$ for half the wavelength, having in mind an experiment of finite height h and rigid vertical boundaries.

Perturbations associated with a single mode are exponential in time, but it is convenient to allow for general time dependence and discover the fastest-growing mode by integrating the linearized equations forward in time. These equations are (see the Appendix)

$$\dot\beta_\theta = \eta(D-k^2)\beta_\theta + kV_A\varphi_\theta + \underline{r\Omega'\beta_r} \tag{2}$$

$$\dot\varphi_\theta = \nu(D-k^2)\varphi_\theta - kV_A\beta_\theta - r^{-1}(r^2\Omega)'\varphi_r \tag{3}$$

$$\dot\beta_r = \eta(D-k^2)\beta_r + kV_A\varphi_r \tag{4}$$

$$\dot\varphi_r = \nu(D-k^2)\varphi_r - kV_A\beta_r + \Pi \tag{5}$$

$$(k^2-D)\Pi = 2\Omega k^2\varphi_\theta \tag{6}$$

The prime in eqs. (2)-(3) means $\partial/\partial r$, and

$$D \equiv \frac{\partial^2}{\partial r^2} + \frac{1}{r}\frac{\partial}{\partial r} - \frac{1}{r^2}.$$

Note that Chandrasekhar (1961) denotes the latter operator by DD_*.

Equations (2)-(3) are the azimuthal components of the induction and euler equations, while (4)-(5) are the corresponding radial components. By eliminating the auxiliary function Π between eqs. (5)-(6), one obtains an equation equivalent to Chandrasekhar's eq. (168), although some differences in sign occur because we have taken perturbations proportional to $\sin kz$ where he took $\cos kz$ and *vice versa*. Our eqs. (2), (3), and (4) correspond to his eqs. (163), (160), and (162), respectively.

The flow is confined between concentric cylinders with radii $r_1 < r_2$. If these are perfectly conducting, the magnetic boundary conditions are

$$\beta_r = 0, \qquad\qquad (r\beta_\theta)' = 0. \tag{7}$$

If perfectly insulating, then (I_n and K_n are modified Bessel functions)

$$\begin{aligned} \frac{\partial}{\partial r}(r\beta_r) &= \beta_r \times \begin{cases} [krI_0(kr)]/I_1(kr) & \text{at } r = r_1 \\ -[krK_0(kr)]/K_1(kr) & \text{at } r = r_2 \end{cases} \\ \beta_\theta &= 0. \end{aligned} \tag{8}$$

The conditions on velocity are

$$\varphi_r = 0, \qquad\qquad \nu\varphi_\theta = 0 = \nu(r\varphi_r)'. \tag{9}$$

We have put the viscosity in the latter two conditions so that φ_θ and $\varphi_z = (r\varphi_r)'/(kr)$ will be unconstrained when the flow is inviscid.

The insulating conditions (8) are not accurate for an experiment of finite height $h = \pi/k$, since they assume a vertically periodic solution for the vacuum field outside the cylinders. The conducting conditions (7) do not have this drawback. In both cases, there will be viscous boundary layers at the top and bottom (unless the end caps rotate differentially), but we expect that the error committed by neglecting those layers is small for $P_{\rm m} \sim 10^{-6}$ and growth times shorter than the Ekman circulation time. In any event, the end caps should be insulating so that no magnetic stress acts upon them.

3. Why the small-$P_{\rm m}$ approximation suppresses the MRI

The underlined term in eq. (2) is the critical one that Chandrasekhar (1961) and subsequent authors neglected on the grounds that $P_{\rm m} \ll 1$. To see that this term is necessary to the MRI, it is useful to reduce eqs. (2)-(6) to a single equation.

For brevity's sake, assume a mode with definite growth rate s, and write $D_k \equiv D - k^2$, $\omega_A \equiv kV_A$. Eq. (4) yields

$$\varphi_r = \omega_A^{-1}(s - \eta D_k)\beta_r \,. \tag{10}$$

Substituting for φ_r in eq. (5), applying D_k, and eliminating $D_k\Pi$ *via* eq. (6), one has

$$\varphi_\theta = -(2\Omega k^2 \omega_A)^{-1} \left[(s-\nu D_k)(s-\eta D_k) + \omega_A^2\right] D_k \beta_r \,. \tag{11}$$

Solving for β_θ from eq. (3) and eliminating φ_θ and φ_r in favor of β_r, one has

$$\begin{aligned} \beta_\theta &= \omega_A^{-2} \left\{ (s-\nu D_k) \frac{1}{2\Omega k^2} \left[(s-\nu D_k)(s-\eta D_k) + \omega_A^2\right] D_k \right. \\ &\quad \left. - \frac{(r^2\Omega)'}{r} (s-\eta D_k) \right\} \beta_r \,. \end{aligned} \tag{12}$$

Using these to eliminate φ_θ and β_θ from eq. (2) yields the desired tenth-order equation:

$$\begin{aligned} \left\{ \left[(s-\nu D_k)(s-\eta D_k) + \omega_A^2\right] \frac{1}{2\Omega} \left[(s-\nu D_k)(s-\eta D_k) + \omega_A^2\right] (-k^{-2} D_k) \right. \\ \left. + (s-\eta D_k) \frac{(r^2\Omega)'}{r} (s-\eta D_k) \right\} \beta_r \;=\; -\omega_A^2 \underline{r\Omega' \beta_r}. \end{aligned} \tag{13}$$

We are interested in Rayleigh-stable cases. Without loss of generality, we may assume that the angular velocity (Ω) and vorticity $[r^{-1}(r^2\Omega)']$ are positive throughout the flow, but the shear ($r\Omega'$) may be negative. Now D_k is clearly negative definite and self adjoint with either of the boundary conditions (7) or (8). In the narrow-gap limit $(r_2 - r_1)/(r_2 + r_1) \to 0$, the angular velocity and vorticity are positive constants. It follows that the operator in braces in the lefthand side of eq. (13) is positive definite for nonnegative real s. Therefore, *at least in the narrow-gap limit, there can be no modes with positive real growth rate when the underlined shear term is neglected and the Rayleigh stability criterion is satisfied.* We interpret this to mean that the MRI is not present.

Previous studies of the time-dependent problem have neglected the time derivatives in the induction equation as well as the underlined term (Chang & Sartory 1967; Chen & Chang 1998); in this case, the operator in question becomes quadratic in s so that the coefficient of Imag(s) is positive-definite for Real(s) > 0, which rules out complex growing modes, *i.e.* overstabilities.

Unfortunately, we cannot draw such strong conclusions in the wide-gap case where Ω and perhaps also $r^{-1}(r^2\Omega)'$ vary significantly with radius. The operator on the left side of eq. (13) is no longer self adjoint in general, because D_k and Ω do not commute. For marginal modes, however,

$$\left\{ \left[\nu D_k^2 + \frac{\omega_A^2}{\eta}\right] \frac{\eta}{2\Omega k^2} \left[\nu D_k^2 + \frac{\omega_A^2}{\eta}\right] \;-\; \eta D_k \frac{(r^2\Omega)'}{r} \right\} \varphi_r \;=\; -\omega_A \underline{r\Omega' \beta_r} \,, \tag{14}$$

in which we have used eq. (10). In this case the problem is only eighth order in radial derivatives if the righthand side is neglected, as noted by Chandrasekhar (1961). More importantly, the operator in these curly braces *is* self adjoint in the interesting special case that

$$\Omega(r) = a + \frac{b}{r^2}, \tag{15}$$

since $r^{-1}(r^2\Omega)' = 2a$ is then constant, and the rest of the operator is symmetrical. Eq. (15) is the angular-velocity profile of a Couette flow in steady state, because it implies a radially constant viscous angular-momentum flux. We conclude that there are no Rayleigh-stable *marginal* modes when the magnetic shear term is neglected, even for wide gaps.

4. Marginal inviscid modes

If $\nu = 0$, then as the growth rate $s \to 0$, eq. (13) reduces to

$$\left[\eta^2 D_k \frac{(r^2\Omega)'}{r} - \frac{\omega_A^4}{2\Omega k^2}\right] D_k\beta_r = -\omega_A^2 \underline{r\Omega'\,\beta_r}\,. \tag{16}$$

Even with the righthand side included, this is only a fourth-order system. Paradoxically, there are six boundary conditions to be satisfied: φ_θ and φ_z are not constrained when $\nu = 0$, but $\varphi_r = 0$ at both boundaries, in addition to a total of four magnetic conditions. For the insulating case (8), the paradox is resolved because eqs. (10) and (12) show that both $\varphi_r = 0$ and $\beta_\theta = 0$ are equivalent to $D_k\beta_r = 0$, so that there are only four independent boundary conditions after all. But in the conducting case (7), we have *via* eqs. (10)-(12) that $\beta_r = D_k\beta_r = (rD_k\beta_r)' = 0$ at both boundaries, and not all six conditions can be satisfied.

The crux of the difficulty is the azimuthal euler equation (3), which reduces to an algebraic relation. At zero viscosity and growth rate, azimuthal force balance requires

$$2\Omega\delta v_r = \frac{B_0}{4\pi\rho}\frac{\partial\delta B_\theta}{\partial z}\,, \tag{17}$$

so that the Lorentz force ($\delta j_r \times B_0$) balances the Coriolis force, which vanishes at the boundary. If the boundary is insulating, then δB_θ ($\propto \delta j_r$) also vanishes. But at conducting boundaries, $\delta B_\theta \neq 0$ ($\delta j_r \neq 0$), so that viscosity must intervene to maintain azimuthal force balance. For small $P_{\rm m}$, the marginal eigenfunction displays a dramatic boundary layer (Fig. 3).

Viscous boundary layers are common in hydrodynamics. Normally they occur because the tangential component of velocity must match that of the boundary itself, even when the viscosity is small (a "no-slip" boundary condition). For conducting cylinders, however, *a boundary layer would occur even if the viscous stress vanished at the boundary*, because of the impossibility of satisfying eq. (17). In the present case, the viscous layer is driven by tangential *magnetic field* (or normal component of current) rather than tangential velocity.

To summarize, the inviscid limit is singular for marginally stable modes. The eigenfunctions become ill-behaved because there are more boundary conditions than radial derivatives to satisfy them, at least for conducting boundaries. The numerical evidence presented below indicates, however, that the locus of marginal stability in the parameter space of equilibria is actually continuous as $P_{\rm m} \to 0$. Hence the relatively simple fourth-order differential equation (16) predicts marginal stability reasonably well when $P_{\rm m}$ is sufficiently small.

5. Numerical results

We have approximated eqs (2)-(6) by finite-difference equations on a radial grid uniformly spaced in $x \equiv \ln r$. The background angular velocity has the form (15), since this is easiest to realize experimentally. The grid spacing Δx must be chosen fine enough so that $\Delta r^2/\nu$ is smaller than the interesting physical timescales in the problem, *viz.* ω_A^{-1} and $(\eta d^2)^{-1}$ (where $d \equiv r_2 - r_1$ is the gap width), otherwise the viscous boundary layer will not be resolved. The minimum number of grid cells $N \sim P_{\rm m}^{-1/2} \sim 10^3$. Our scheme has second-order spatial accuracy, even at the the boundaries.

To ensure numerical stability, we use fully implicit time differencing. Spatial differences are written in terms of the unknown dependent variables at the new time step, so that a large linear system must be solved. Actually, our finite-difference matrix is band diagonal with 10 nonzero codiagonals in each of $5N$ rows, and it is independent of time step. We perform LU decomposition at the start of the evolution so that only the back substitution must be performed anew at each step.

When a growing mode is present, it eventually dominates. Then the perturbation in radial magnetic field at successive time steps t_n and $t_{n+1} = t_n + \Delta t$ are related by, for example,

$$(1 - \hat{s}\Delta t)\,\hat{\beta}_r(x_j, t_{j+1}) = \hat{\beta}_r(x_j, t_j), \tag{18}$$

if $\hat{s} > 0$ is the appropriate eigenvalue of the matrix defined by the spatial difference scheme and therefore an estimate of the physical growth rate, and $\hat{\beta}_r$ is the corresponding eigenvector. Given $\hat{\beta}_r(x_j, t_j)$ and $\hat{\beta}_r(x_j, t_{j+1})$, we can compute $\hat{s}$ from eq. (18) without any truncation error in Δt as long as $\hat{s}\Delta t < 1$. The eigenfunctions are similarly independent of Δt. This is advantageous close to marginal stability where $\hat{s}$ is small. Our procedure is equivalent to finding the most-positive eigenvalue of the time-evolution matrix by inverse iteration. By extending eq. (18) to a three-term recurrence relation, we have allowed for complex eigenvalues. But in practice, all of our growing modes appear to have purely real values of $\hat{s}$. Of course, our method is not immune to *spatial* truncation errors; these are $O(\Delta x^2)$ because we use second-order spatial differencing.

Our initial-value code can treat slightly stable cases as well as unstable ones. By interpolation, we find parameters for marginal stability. Results are shown in Figs. (1) & (2) for material properties approximating liquid gallium, *viz.* $\rho = 6\,{\rm g\ cm^{-3}}$, $\eta = 2000\,{\rm cm^2 s^{-1}}$ and $P_{\rm m} = 1.6 \times 10^{-6}$.

Marginal stability defines one constraint among the eight parameters defining the Couette flow: η, ν, r_1, r_2, k, Ω_1, Ω_2, and V_A. Six independent dimensionless combinations of these can be formed. The magnetic Prandtl number $P_{\rm m} \equiv \nu/\eta$ is one of these. The aspect ratio

$$A \equiv \frac{r_2 + r_1}{d}\ , \tag{19}$$

and the elongation of the toroidal cross section,

$$\epsilon \equiv \frac{h}{d} \tag{20}$$

define the geometry, where $d \equiv r_2 - r_1$ is the gap width and $h \equiv \pi/k$ is half the vertical wavelength. It turns out that the magnetic eigenfunctions β_r and β_θ of the most unstable mode have a roughly parabolic dependence on r, and since one or the other vanishes at both boundaries, the effective horizontal wavenumber is $\approx \pi/d$. The total wavenumber is then

$$K \equiv \left(k^2 + \frac{\pi^2}{d^2} \right)^{1/2} = \frac{\pi}{h} \sqrt{1 + \epsilon^2}. \tag{21}$$

The Lundquist number

$$S \equiv \frac{k V_A}{\eta K^2} = \frac{V_A h}{2\pi\eta} \, \frac{2}{\epsilon^2 + 1} \tag{22}$$

scales the Alfvén frequency against the magnetic diffusion rate ηK^2. In astrophysics, S is often called "magnetic Reynolds number." The plasma community generally reserves the latter term for a quantity involving fluid velocity, so we define the local magnetic Reynolds number by

$$R_{\rm m}(r) \equiv \frac{\Omega}{\eta K^2}. \tag{23}$$

The viscous Reynolds number is of course $R_{\rm m}/P_{\rm m}$. The dimensionless vorticity

$$\zeta(r) \equiv \frac{(r^2\Omega)'}{r\Omega} \tag{24}$$

parametrizes the angular momentum gradient, and the Rayleigh stability criterion is simply $\zeta(r) \geq 0$. In the astrophysical literature, the radial variation of angular velocity is often described by an index

$$q \equiv -\frac{d \ln \Omega}{d \ln r} \qquad \text{so that} \qquad \zeta = 2 - q.$$

Of course, $\zeta = 2$ and $q = 0$ in a uniformly rotating flow.

When the aspect ratio is modest, $R_{\rm m}$ and ζ may vary considerably across the gap, and it is useful to define mean values of these dimensionless parameters. Following Paper I, we introduce $\bar\Omega \equiv \sqrt{\Omega_1 \Omega_2}$ and

$$\bar R_{\rm m} \equiv \frac{\bar\Omega}{\eta K^2}, \qquad \bar\zeta \equiv \frac{2(r_2^2\Omega_2 - r_1^2\Omega_1)}{(r_2^2 - r_1^2)\bar\Omega} \tag{25}$$

The locus of marginal stability is actually a hypersurface in the space $(P_{\rm m}, A, \epsilon, \bar\zeta, S, \bar R_{\rm m})$. The curves in Figs. (1)-(2) are cuts through this locus at constant values of the first four parameters: $P_{\rm m} = 0$ and $P_{\rm m} = 1.6 \times 10^{-6}$; $A = \epsilon = 1$; and two positive values of ζ as indicated. The curves are drawn in physical units for the density and diffusivity of gallium.

The inviscid results shown in in these figures were calculated by an independent numerical method based on eq. (16), which we have unpacked into a pair of second-order equations [using eq. (12) with $s, \nu \to 0$]:

$$D_k \beta_r \;=\; \frac{r\omega_A^2}{\eta (r^2\Omega)'} \, \beta_\theta \qquad\qquad = \; K^2 \, \frac{S^2}{\zeta R_{\rm m}} \, \beta_\theta, \tag{26}$$

$$D_k\beta_\theta \;=\; \frac{\omega_A^4\, r}{2\Omega(r^2\Omega)'\,\eta^2 k^2}\,\beta_\theta \;-\; \frac{r\Omega'}{\eta}\beta_r \;=\; K^2\left[\frac{(1+\epsilon^2)S^4}{2\zeta R_{\rm m}^2}\,\beta_\theta + (2-\zeta)R_{\rm m}\beta_r\right], \qquad (27)$$

together with the magnetic boundary conditions (7) or (8). Because of the large magnetic diffusivity, the magnetic variables are very well-behaved, so that this fourth-order system can be solved efficiently by a shooting method.

Comparing Figs. 3 and 4, one sees that viscosity is more important for conducting boundary conditions than for insulating ones. In the conducting case, φ_r and β_θ are nearly proportional to one another throughout most of the flow [Fig. 3]. This follows from eq. (3) in the limit $s, \nu \to 0$, as we discussed in §4. Since the radial velocity perturbation ($\propto \varphi_r$) must vanish at the wall but the azimuthal magnetic perturbation ($\propto \beta_\theta$) does not, there is a thin boundary layer in which viscous stress balances the azimuthal magnetic force. The righthand panel shows that the boundary layer is well resolved by these calculations, which use 4000 grid points uniformly spaced in $\ln r$ across the gap. At an insulating boundary, on the other hand, β_θ vanishes with φ_r, and this leads to a much less dramatic viscous layer (Fig. 4).

The narrow-gap limit $A \to \infty$ is experimentally impractical but theoretically important. Fig. 5 shows eigenfunctions and curves of marginal stability and in this limit. Because of the boundary conditions, the eigenfunctions cannot be sinusoidal in r or $x \equiv (r-r_1)/d$, even though the equations of motion have elementary solutions of this form. The fourth-order inviscid system (26)-(27) has four roots for the radial wavenumber (or two if sign is ignored) at given parameters $(\epsilon, S, R_{\rm m}, \zeta)$ of the equilibrium, which are constant across the gap. (Note K is not an independent parameter, since $Kd = \sqrt{\epsilon^2+1}$.) The solutions satisfying the boundary conditions are linear combinations of four complex exponentials, each containing one of these wavenumbers, and the parameters $(\epsilon, S, R_{\rm m}, \zeta)$ must satisfy one constraint in order that a solution exist. If, however, one simply sets $k_r = \pi/d$ in hopes of obtaining an approximate constraint, then $D_k \to -K^2$ and eqs. (26)-(27) or (16) would yield

$$R_{\rm m}^2 = S^2\frac{1+\epsilon^2}{2(2-\zeta-\zeta S^{-2})}. \qquad (28)$$

This corresponds to the dispersion relation for marginal modes obtained in Paper I from a local WKB analysis with a ratio ϵ of vertical to horizontal wavelength. Evidently there exists a minimum Lundquist number for instability,

$$S_{\rm min} = \sqrt{\frac{\zeta}{2-\zeta}}, \qquad (29)$$

and in the opposite limit of large S,

$$\frac{R_{\rm m}}{S} = \frac{\Omega}{kV_A} \approx \sqrt{\frac{1+\epsilon^2}{2(2-\zeta)}}. \qquad (30)$$

Fig. (5) shows that the predictions (28)-(30) are qualitatively correct.

Numerical growth rates are given in Table 1 for two representative angular-velocity profiles, both with $r_2 = 3r_1 = 15\,{\rm cm}$, $h = 10\,{\rm cm}$, and the material properties of gallium. The first case has

$\bar{\zeta} = 0.063$ and hence is Rayleigh-stable. The second has $\bar{\zeta} = -0.019$, so that the Rayleigh instability occurs at zero field strength. Growth rates are shown for conducting and insulating radial boundary conditions. Larger fields are required to initiate and to quench MRI with insulating boundaries than with conducting ones, presumably because perturbed lines of force expand past insulating walls into a volume slightly larger than the Couette flow itself. The final column of this table shows growth rates computed from the algebraic local dispersion relation given by in Paper I. Once again the WKB analysis predicts the global growth rates remarkably well, even though the wavelengths involved are actually larger than the gap width, and the angular velocity and shear rate vary by a factor ≈ 9 across the gap.

Figures (6) and (7) show two-dimensional cross sections of selected modes from Table 1. The flux and stream functions are related to the poloidal perturbations by

$$\frac{\delta \mathbf{B}_P}{\sqrt{4\pi\rho}} = \boldsymbol{\nabla}\theta \times \boldsymbol{\nabla}\chi\,, \qquad \delta \mathbf{v}_P = \boldsymbol{\nabla}\theta \times \boldsymbol{\nabla}\psi\,. \tag{31}$$

In all cases, the poloidal velocity field consists of a single roll. The effect of the choice of boundary conditions is seen most clearly in the toroidal perturbations. In the first part of Fig. (6) and the second part of Fig. (7), it looks as though δv_θ does not vanish at the inner boundary; in fact it does vanish, but the viscous boundary layer is too small to be resolved by these plots. The first part of Fig. (7) does not show this behavior because the magnetic forces are absent; this mode is a classical hydromagnetic centrifugal instability. A boundary layer of the ordinary nonmagnetic variety occurs in δv_z. The corresponding magnetized case shown in the second part of the figure has a magnetically-driven boundary layer similar to that of the Rayleigh-stable flows.

6. Summary and discussion

We have presented a global linear stability analysis for magnetized Couette flow, including the dissipative effects of viscosity and resistivity, in regimes where magnetorotational instability (MRI) is possible. In view of the actual properties of liquid metals, and for plausible experimental lengthscales, resistivity is the main obstacle that must be overcome to demonstrate MRI. Previous theoretical studies of magnetized Couette flow have focused on the problem of suppressing Rayleigh instability with a magnetic field, and they have simplified the induction equations so as to reduce the number of radial and time derivatives in the problem. Such approximations may be adequate for the regime of interest to those studies, but they will not do if one is interested in MRI. Therefore we have worked with the full induction equations.

Particular attention has been given to marginal stability. All of our numerical evidence indicates that exchange of stability occurs at vanishing complex growth rates; we have not encountered any overstable modes. In the inviscid limit of marginal stability, the number of radial derivatives reduces from ten to four, but the velocity perturbations become singular at conducting boundaries. The dominant singularity arises from an unbalanced tangential magnetic force, not from the usual

pressure and inertial effects that cause boundary layers in unmagnetized fluids. Despite these complications, the inviscid approximation predicts the locus of marginal stability reasonably well for liquid metals.

Solving the linearized initial-value problem by finite-differences, we have calculated growth rates and stability boundaries for a liquid metal approximating gallium in an experimentally plausible geometry. For easier comparison with other theoretical work, we have also made calculations in the narrow-gap limit and expressed our results in the dimensionless coordinates of Lundquist number and magnetic Reynolds number.

Remarkably, the growth rates are reasonably well predicted by a simple WKB approximation even though the WKB modes do not satisfy the boundary conditions and have a radial wavelength twice the gap width, and even when the rotation rate varies by an order of magnitude across the gap. We conclude from this that the algebraic WKB dispersion relation can be used for preliminary experimental design, at least for aspect ratios no more extreme than considered here ($r_2 : r_1 = 3 : 1$).

There are good reasons to attempt an MRI experiment. First, one can hardly exaggerate the importance of this instability: few or no plausible alternative explanations exist for the dissipation of orbital energy in accretion disks, which are fundamental to so many of the most energetic sources known in the universe. Yet all present knowledge of the instability is purely theoretical, based as it is on linear analysis and computer simulation; the constraints provided by astronomical observations are very indirect. It is prudent to put these theories to a laboratory test.

Secondly, computer speed limits the range of spatial scales that can be modeled in the simulations. Barring unforseen algorithmic breakthroughs, the smallest resolvable scale in a three-dimensional simulation improves only as the fourth root of the rate of arithmetic operations. Here it must be acknowledged that the large magnetic diffusivity of liquid metals severely limits the number of degrees of freedom in the magnetic field that can be excited. The simulations are well ahead of any forseeable experiment in this respect. In fact, simulations indicate that magnetic Reynolds numbers and Lundquist numbers at least 100 times larger than the minimum necessary for linear instability are required for dynamo action in the absence of an externally imposed field parallel to the rotation axis (Fleming, Stone, & Hawley 2000). On the other hand, the viscous Reynolds number of such an experiment would be $R_\mathrm{e} \gtrsim 10^6$, a value still out of reach of direct numerical simulations. Also, small R_m need not restrict the experiment to linear behaviors. In the local disk simulations of Fleming, Stone, & Hawley (2000) at about twice the minimum R_m for linear MRI, a violently fluctuating nonlinear state was reached in which the time-averaged magnetic energy was about 25 times larger than that of the externally imposed field.

Although large R_m is the rule in astrophysics, the dimensionless parameters of some systems may be similar to those of our proposed experiment, *viz.* R_m and S of order unity, R_e very large, and an externally imposed field. Such systems include the inner parts of relatively cool disks (protostellar disks and quiescent cataclysmic variables, for example) around stars with their own magnetic moments (Gammie 1996; Gammie & Menou 1998).

Lastly, relatively little laboratory MHD work has been done in which the inertia of the fluid is important (large plasma β). The experimental field appears somewhat underdeveloped when measured against its potential importance to geophysics and astrophysics. Because it promises to be achievable at fairly modest cost in a classic experimental framework (Couette flow), MRI is a good place to start.

This work was supported by the U.S. Department of Energy [H.J.] and by NASA grant NAG5-8385 [J.G.]

A. Derivation of linearized equations

For completeness, eqs. (2)-(6) are derived here, although much the same derivation can be found in Chandrasekhar (1961). The equations of incompressible MHD are

$$\begin{aligned} \dot{\mathbf{B}} + \mathbf{v}\cdot\boldsymbol{\nabla}\mathbf{B} - \mathbf{B}\cdot\boldsymbol{\nabla}\mathbf{v} &= \eta\nabla^2\mathbf{B}, \qquad \boldsymbol{\nabla}\cdot\mathbf{B} = 0, \\ \dot{\mathbf{v}} + \mathbf{v}\cdot\boldsymbol{\nabla}\mathbf{v} + \rho^{-1}\boldsymbol{\nabla}P - \frac{\mathbf{B}\cdot\boldsymbol{\nabla}\mathbf{B}}{4\pi\rho} &= \nu\nabla^2\mathbf{v}, \qquad \boldsymbol{\nabla}\cdot\mathbf{v} = 0, \end{aligned}$$

in which $P \equiv p + \mathbf{B}^2/8\pi$, is the hydrodynamic plus magnetic pressure. In cylindrical coordinates, near an equilibrium $\mathbf{B}_0 = B\mathbf{e}_z$ = constant and $\mathbf{v}_0 = r\Omega(r)\mathbf{e}_\theta$, linearized axisymmetric perturbations $\delta\mathbf{v}$ and $\delta\mathbf{B}$ satisfy

$$\delta\dot{B}_r - B\partial_z\delta v_r = \eta(\partial_r\partial_r^\dagger + \partial_z^2)\delta B_r, \tag{A1}$$

$$\delta\dot{B}_\theta - B\partial_z\delta v_\theta - \delta B_r r\partial_r\Omega = \eta(\partial_r\partial_r^\dagger + \partial_z^2)\delta B_\theta, \tag{A2}$$

$$\delta\dot{v}_r - 2\Omega\delta v_\theta + \partial_r\frac{\delta P}{\rho} - \frac{B}{4\pi\rho}\partial_z\delta B_r = \nu(\partial_r\partial_r^\dagger + \partial_z^2)\delta v_r, \tag{A3}$$

$$\delta\dot{v}_\theta + \delta v_r\partial_r^\dagger(r\Omega) - \frac{B}{4\pi\rho}\partial_z\delta B_\theta = \nu(\partial_r\partial_r^\dagger + \partial_z^2)\delta v_\theta, \tag{A4}$$

$$\delta\dot{v}_z + \partial_z\frac{\delta P}{\rho} - \frac{B}{4\pi\rho}\partial_z\delta B_z = \nu(\partial_r^\dagger\partial_r + \partial_z^2)\delta v_z, \tag{A5}$$

$$\partial_r^\dagger\delta B_r + \partial_z\delta B_z = 0, \tag{A6}$$

$$\partial_r^\dagger\delta v_r + \partial_z\delta v_z = 0, \tag{A7}$$

in which the dot denotes $\partial/\partial t$, and other recurring operators are

$$\partial_z \equiv \frac{\partial}{\partial z}\,, \quad \partial_r \equiv \frac{\partial}{\partial r}\,, \quad \partial_r^\dagger \equiv \frac{\partial}{\partial r} + \frac{1}{r}\,.$$

Eqs. (A3) & (A5) presume that ρ, like η and ν, is spatially constant. Applying $\partial_r^\dagger$ to eq. (A3) and ∂_z to eq. (A5) and summing the results, one finds that

$$(\partial_r^\dagger\partial_r + \partial_z^2)\frac{\delta P}{\rho} = \partial_r^\dagger(2\Omega\delta v_\theta),$$

in view of eqs. (A6) & (A7). With another application of ∂_r, this becomes

$$(\partial_r \partial_r^\dagger + \partial_z^2)\Pi = \partial_z^2(2\Omega\delta v_\theta), \qquad \text{where } \Pi \equiv 2\Omega\delta v_\theta - \partial_r \frac{\delta P}{\rho} , \tag{A8}$$

so that the radial euler equation (A3) can be stated as

$$\delta\dot{v}_r - \Pi - \frac{B}{4\pi\rho}\partial_z \delta B_r = \nu(\partial_r\partial_r^\dagger + \partial_z^2)\delta v_r. \tag{A9}$$

With the z dependences given by eq. (1) for the linearized quantities, eqs. (A2), (A4), (A1), (A9), and (A8) reduce to eqs. (2), (3), (4), (5), and (6), respectively.

REFERENCES

Balbus, S. A. & Hawley, J. F. 1991 *Astrophys. J.* **376**, 214.

Balbus, S. A. & Hawley, J. F. 1992 *Astrophys. J.* **392**, 662.

Brahme, A. 1970 *Physica Scripta* **2**, 108.

Chandrasekhar, S. 1960 *Proc. Nat. Acad. Sci.* **46**, 253.

Chandrasekhar, S. 1961 *Hydrodynamic and Hydromagnetic Stability.* (London: Oxford University Press).

Chang, T. S. & Sartory, W. K. 1967 *Proc. R. Soc. Lond.* **A 301**, 451.

Chen, C.-K. & Chang, M. H. 1998 *J. Fluid Mech.* **366**, 135.

Donnelly, R. J. & Caldwell, D. R. 1964 *J. Fluid Mech.* **19**, 257.

Donnelly, R. J. & Ozima, M. 1960 *Phys. Rev. Lett.* **4** (10), 497.

Donnelly, R. J. & Ozima, M. 1960 *Proc. R. Soc. Lond.* **A 266**, 272.

Fleming, T.P., Stone, J.M., Hawley, J.F. *ApJ,* **530**, 464.

Gammie, C. F. 1996 *ApJ,* **457**, 356.

Gammie, C. F. & Menou, K. 1998 *ApJ,* **492**, L75.

Hassard, B. D., Chang, T. S. & Ludford, G. S. S. 1972 *Proc. R. Soc. London* **A 327**, 269.

Ji, H., Goodman, J., & Kageyama, A. 2001 `astro-ph/0103226` [Paper I].

Terquem, C. & Papaloizou, J. C. B. 1996 *Mon. Not. R. Astr. Soc.* **279**, 767.

Soundalgekar, V. M., Ali, M. A., & Takhar, H. S. 1994 *Int. J. Energy Res.* **18**, 689.

Takhar, H. S., Ali, M. A., & Soundalgekar, V. M. 1994 *Appl. Sci. Res.* **48**, 1.

Vislovich, A. N., Novikov, V. A., & Sinitsyn, V. A. 1986 *J. Appl. Mech. Tech. Phys.* **27** (1), 72.

Velikhov, E. P. 1959 *Sov. Phys. JETP* **36** (2), no. 5, 995.

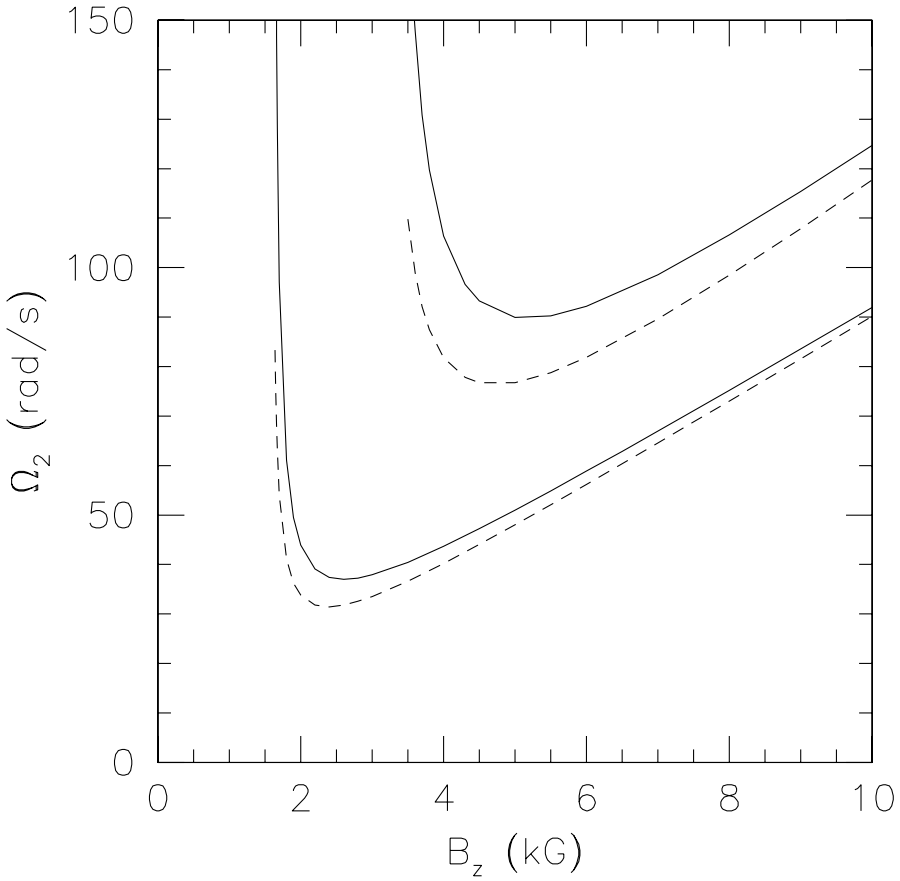

Fig. 1.— Marginal stability for liquid gallium Couette flow between conducting cylinders of radii $r_1 = 5\,\mathrm{cm}$, $r_2 = 15\,\mathrm{cm}$, and height $h = 10\,\mathrm{cm}$. Solid lines computed from eqs. (2)-(6); dashed from inviscid approximation (26)-(27). Lower curves for dimensionless vorticity $\zeta = 2/11$, upper ones for $\zeta = 4/7$. Instability occurs above the curves. In dimensionless parameters, $S \approx 0.92(B/10\,kG)$; and $\bar{R}_\mathrm{m} \approx 0.66(\Omega_2/100\,\mathrm{rad\ s^{-1}})$ (upper curves), $\bar{R}_\mathrm{m} \approx 0.73(\Omega_2/100\,\mathrm{rad\ s^{-1}})$ (lower).

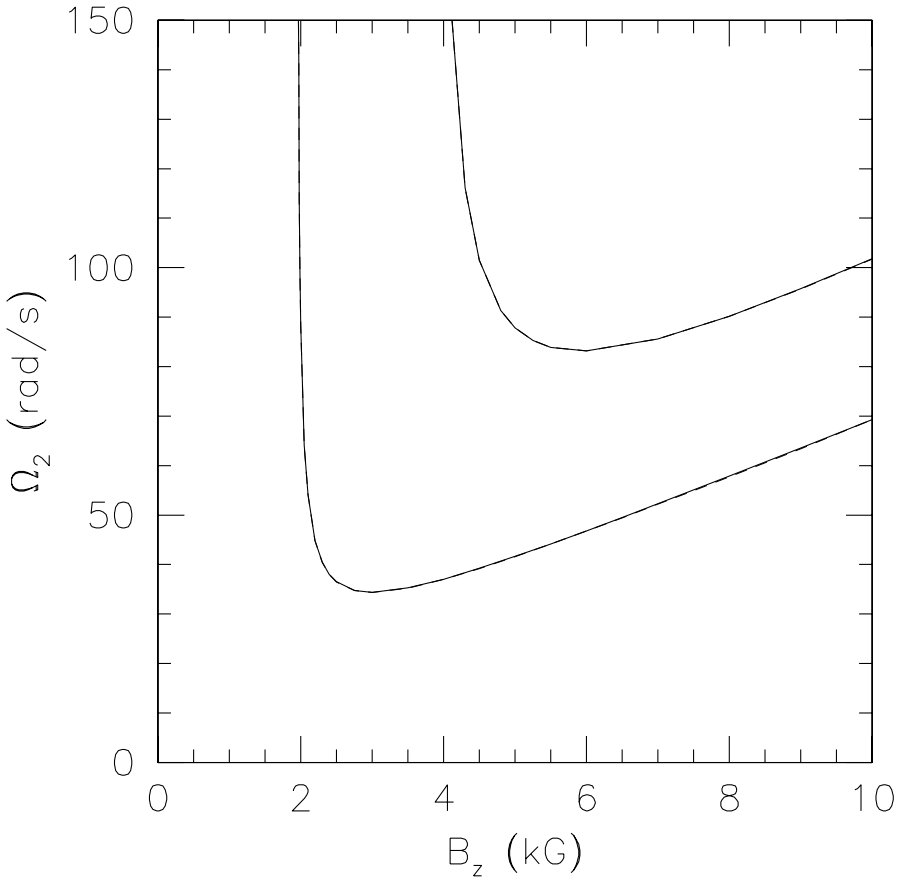

Fig. 2.— Like Fig. (1), but for insulating cylinders (8). Viscous and inviscid results differ by less than the line thickness.

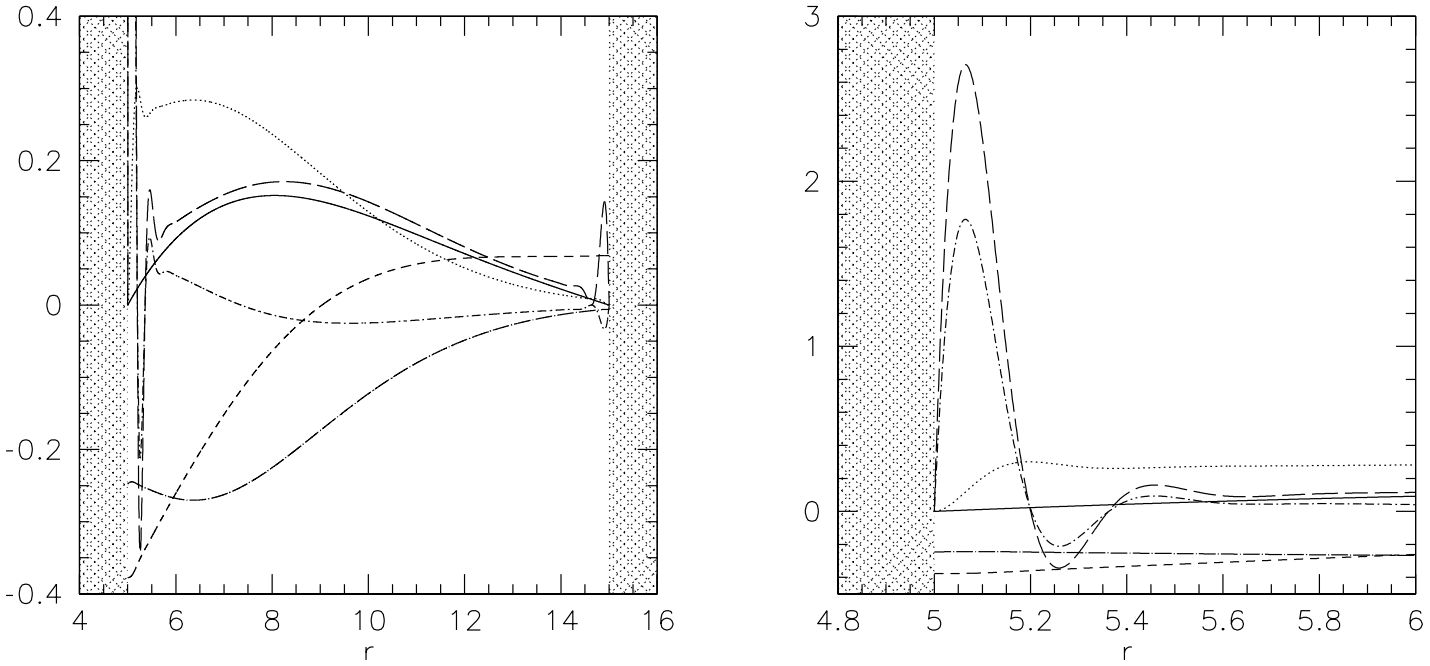

Fig. 3.— Global and closeup views of marginal eigenmode with conducting boundaries. $B = 3\,\mathrm{kG}$, $\Omega_1 = 314.$, $\Omega_2 = 37.9$ rad s^{-1} & $\bar{\zeta} = 0.0632$. Solid curve: β_r. Short-dashed: β_z Dot-long-dashed: $\beta_\theta \times 5$. Dotted: $\varphi_r \times 1/3$. Long-dashed: φ_θ. Dot-short-dashed: $\varphi_z \times 0.07$.

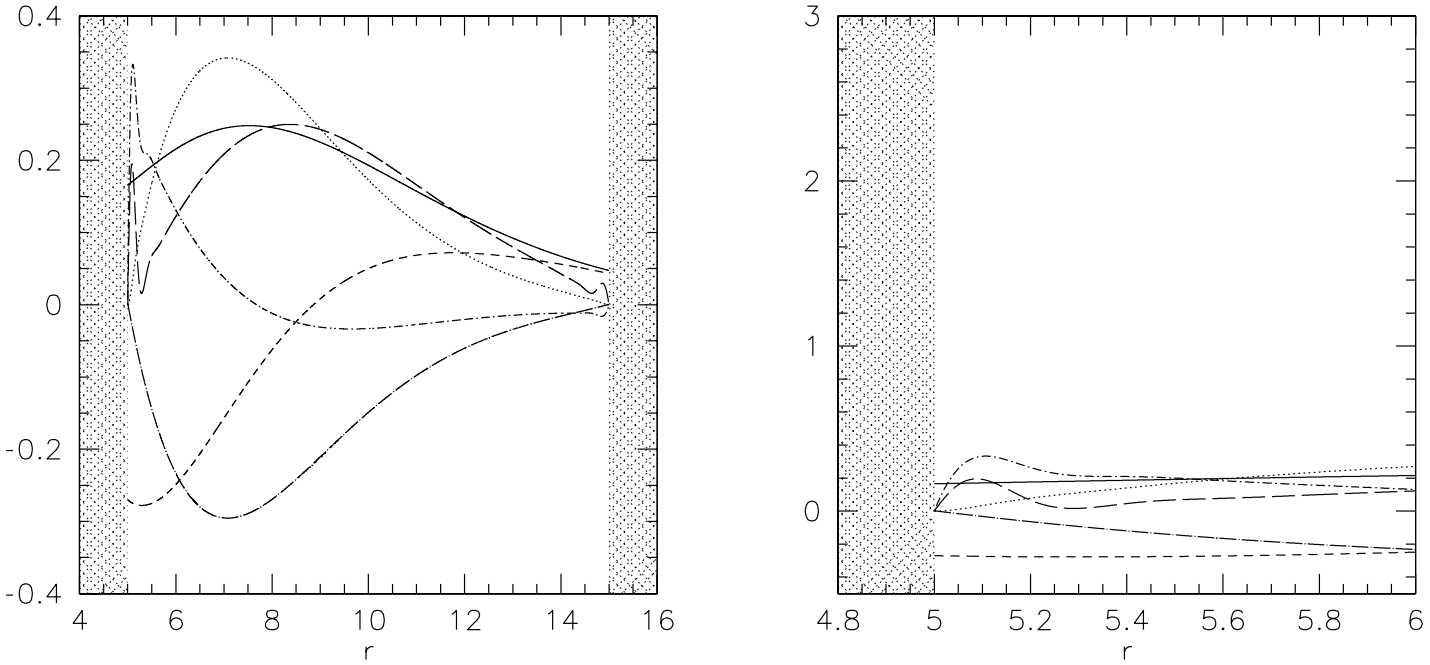

Fig. 4.— Like Fig. 3 but for insulating boundaries and $\Omega_1 = 284.$, $\Omega_2 = 34.4$ rad s^{-1}, $\bar{\zeta} = 0.0632$.

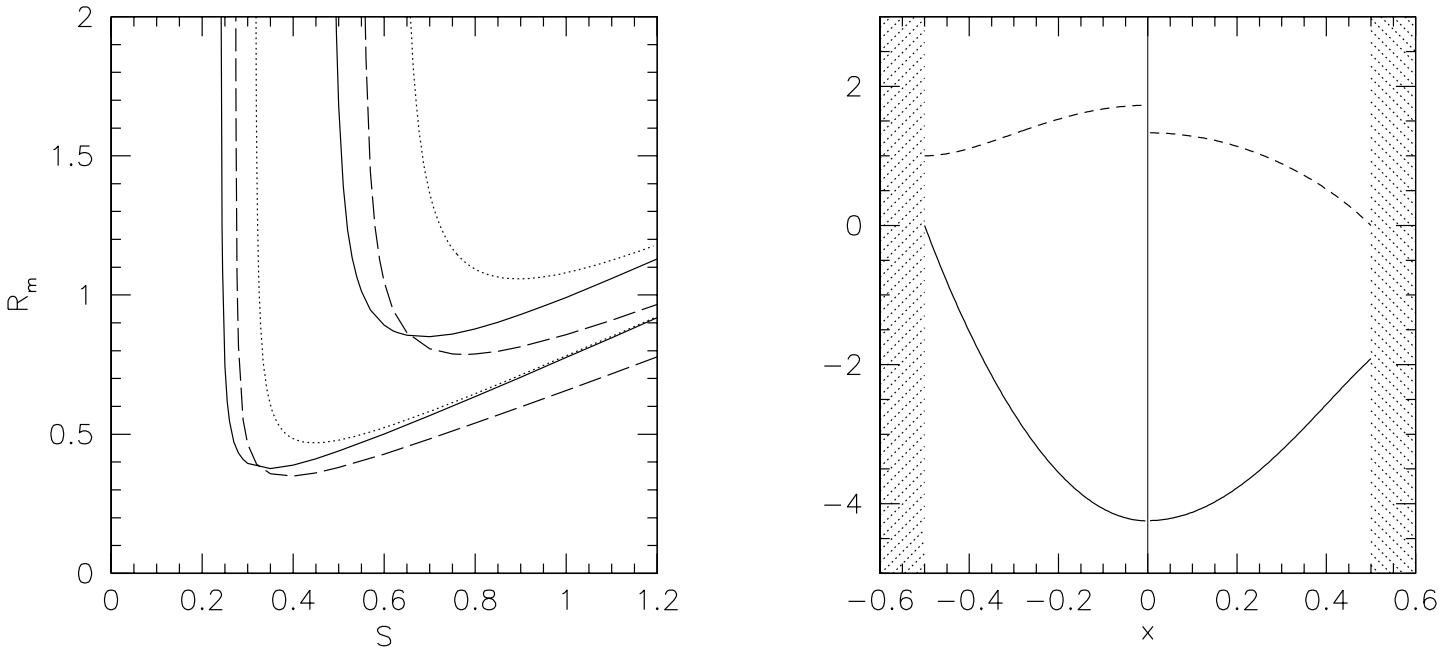

Fig. 5.— Narrow-gap modes for $P_{\rm m} = 0$ and $\epsilon = 1$. *Left panel:* Curves of marginal stability for $\zeta = 2/11$ (lower curves) and $\zeta = 4/7$ (upper). Solid line for conducting walls, dashed for insulating, and dotted for local approximation (28). *Right panel:* Narrow-gap eigenfunctions β_r (solid curves) and β_θ (dashed), for $\zeta = 2/11$ and $S = 0.4$. Since eigenfunctions are symmetric about center of gap ($x = 0$), only half of each is shown: conducting on left, insulating on right.

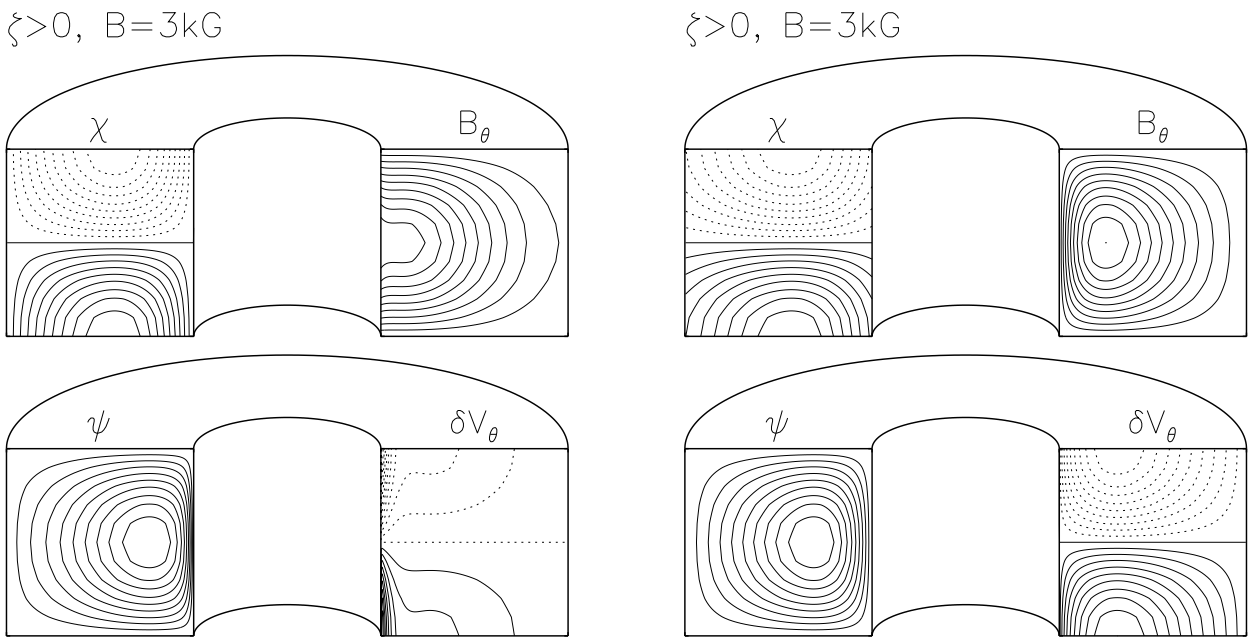

Fig. 6.— Visualizations of the MRI eigenmodes for the Rayleigh-stable cases from Table 1 at $B_{z,0} = 3$ kG. *Left*: conducting boundaries. *Right*: insulating. Solid and dotted lines indicate positive and negative values, respectively. See eq. (31) for definitions of flux and stream functions χ, ψ.

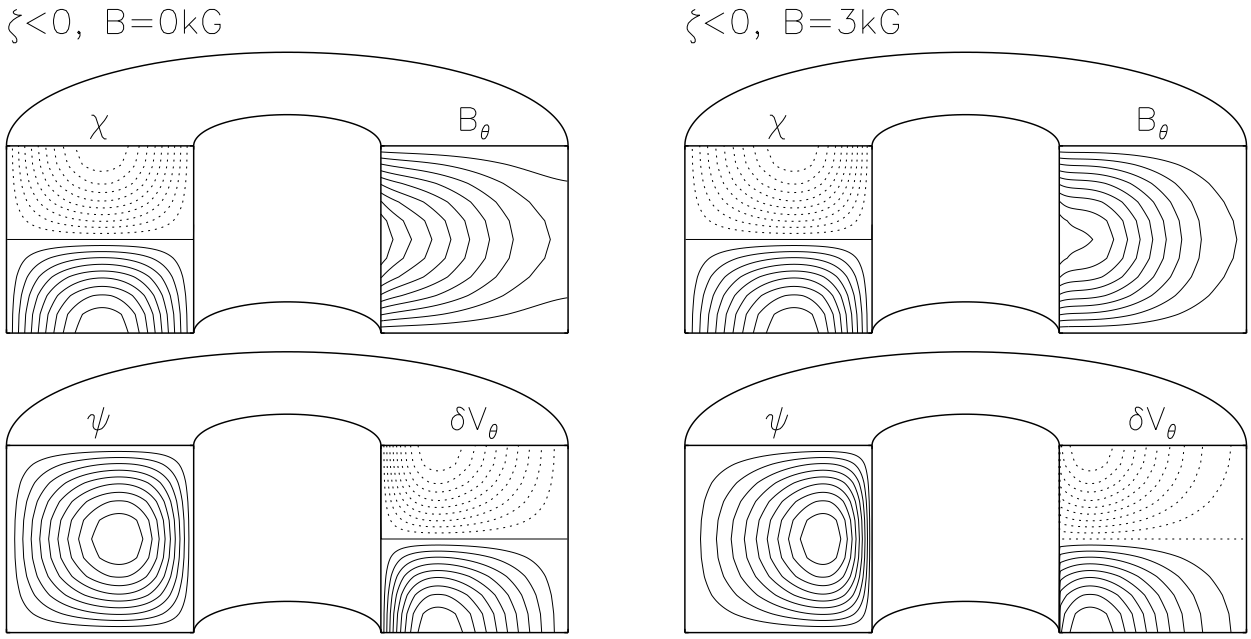

Fig. 7.— Rayleigh-unstable cases from Table 1 at of $B_{z,0} = 0$ kG (left) and 3 kG (right), both with conducting boundaries.

Table 1. Growth rates in gallium

$\Omega_1 = 413.6,\ \Omega_2 = \ 50.$ rad s^{-1}

B_z [G]	*conducting* [s^{-1}]	*insulating* [s^{-1}]	*local* [s^{-1}]
1893.	0.00	—	—
2135.	5.35	0.00	—
2500.	9.46	6.46	6.55
3000.	11.50	10.83	10.48
3500.	10.96	12.66	11.36
4000.	8.42	12.84	9.99
4500.	4.16	11.78	6.63
4868.	0.00	10.38	2.91
5500.	—	7.10	—
6000.	—	3.97	—
6588.	—	0.00	—

$\Omega_1 = 377.0,\ \Omega_2 = \ 40.84$ [rad s^{-1}]

B_z	*conducting*	*insulating*	*local*
0.	16.07	16.07	17.11
500.	17.46	17.00	17.98
1000.	20.10	19.04	19.85
1500.	22.23	21.07	21.58
2000.	23.20	22.50	22.49
3000.	21.13	22.83	20.78
4000.	14.04	19.82	13.50
5000.	4.219	14.38	—
5500.	1.438	11.22	—
6000.	—	8.093	—
6500.	—	5.261	—
7000.	—	2.987	—
8000.	—	.8246	—
9000.	—	.4272	—
10000.	—	.2131	—
11000.	—	3.614e-2	—
11220.	—	0.	—